Theory of scanning tunneling spectroscopy of fullerene peapods

C. L. Kane,[1,3] E. J. Mele,[1,3] A. T. Johnson,[1,3] D. E. Luzzi,[2,3] B. W. Smith,[2,3] D. J. Hornbaker,[4] and A. Yazdani[4]
[1]*Department of Physics, University of Pennsylvania, Philadelphia, Pennsylvania 19104-6396*
[2]*Department of Materials Science and Engineering, University of Pennsylvania, Philadelphia, Pennsylvania 19104-6396*
[3]*Laboratory for Research on the Structure of Matter, University of Pennsylvania, Philadelphia, Pennsylvania 19104-6396*
[4]*Department of Physics and Frederick Seitz Materials Research Laboratory, University of Illinois, Urbana-Champaign, Illinois 61801*
(Received 4 June 2002; revised manuscript received 15 October 2002; published 31 December 2002)

A theory for the hybridization of tube and encapsulant derived electronic states is developed for fullerene peapods: carbon nanotubes encapsulating molecular C_{60}. The interaction between tube and encapsulant is constrained by symmetry and it is studied using a long-wavelength theory of the tube states and a nearly free particle theory of the ball orbitals. Calculations of the local densities of states, resolved in energy and position, are obtained for the gapped bands of a nanotube interacting with a single encapsulated fullerene, with an encapsulated dimer, and with a periodic fullerene peapod lattice. The calculations identify features in the bound state and scattering spectra of the tube produced by hybridization with the encapsulant. For the peapod lattice we identify (a) a narrow defect induced electronic band, (b) a hybridization gap resulting from the strong mixing of tube and ball degrees of freedom, and (c) Bragg gaps produced by electron motion in a periodic defect potential. The theory provides a good description of the prominent features of the measured electronic spectra of fullerene peapods obtained by low-temperature scanning tunneling microscopy.

DOI: 10.1103/PhysRevB.66.235423 PACS number(s): 73.63.Fg, 82.37.Gk, 73.63.−b, 85.35.−p

I. INTRODUCTION

A carbon nanotube is a sheet of graphite wrapped in the shape of a seamless cylinder.[1,2] Nanotubes can be grown with diameters as small as a nanometer, with lengths up to tens of microns, and in multiwall or single wall (SWNT) forms. SWNT's of pure carbon occur in either conducting or semiconducting species, where the variation in their electronic behavior is determined geometrically by the direction along which the graphene sheet is wrapped to form the cylinder.[2–6] There has been considerable progress in the development of new nanometer scale electronic devices based on these structures.[7]

At the same time there is interest in combining carbon nanotubes with other molecular species that can modify their electronic and (or) structural properties. In a seminal paper, Smith, Monthioux, and Luzzi showed that molecular C_{60} (buckyballs) could be incorporated into SWNT's that had been purified in an acid solution, a process that leaves perforations in the tube sidewalls.[8] Subsequent annealing of these structures repairs the external surfaces, encapsulating buckyballs within the tube to form a hybrid all carbon species nicknamed ''peapods.'' In a recent paper we reported the first imaging *and* electronic spectroscopy of nanotube peapods using low-temperature scanning tunneling microscopy,[9] showing that electronic states on the carbon nanotube surface are modified by their hybridization with the electronic orbitals on the encapsulated C_{60}. In these experiments the mixing was observed to be most effective with the lowest unoccupied molecular orbitals of the buckyball. Electronic spectroscopy using the differential tunneling conductance clearly identifies new features in the electronic spectrum of the hybridized system that are not found in the individual subsystems. Strikingly, the differential conductance shows a suppression of the tunneling conductance in a narrow range of energy (a hybridization gap) in which the nanotube states and buckyball orbitals are strongly mixed.

In this paper, we present a theoretical analysis of the data reported earlier in Hornbaker *et al.* Our analysis requires a model for the electronic states on the nanotube sidewalls, a model for the molecular orbitals on the buckyball, and a theory for their interaction. The physics of the former two systems has been well developed over the last few years.[3–6] This paper applies a long-wavelength theory to describe the relevant tube degrees of freedom,[6] and the analogous nearly free-electron theory for the molecular orbitals of the isolated buckyball.[10] Brief reviews of the salient features of these two models are given in Secs. II and III, respectively. Our model for the hybridization of the tube and ball degrees of freedom exploits the symmetries of these low-energy models for the tube and ball electronic states and is presented in Sec. IV. The remainder of the paper is devoted for developing a scattering formalism to describe the effect of the encapsulant on the nanotube electronic degrees of freedom. We develop the theory of the electronic spectrum of the saturated peapod lattice by first studying the scattering properties of encapsulated isolated buckyballs and buckyball dimers in Sec. V. The electronic structure of the ordered peapod lattice is then studied in Sec. VI by constructing and solving a variant of the Kronig Penney model for this structure. Section VII provides a comparison of theory and experiment, and in Sec. VIII we discuss some remaining discrepancies between theory and experiment and directions for future work.

II. ELECTRONIC STATES OF SWNT'S

A. Long wavelength theory of the graphene sheet

The low-energy electronic structure of a single wall carbon nanotube can be studied using a tight binding model in which π electrons hop between the nearest-neighbor sites of a two-dimensional honeycomb lattice that is wrapped along a

specified crystallographic direction.[2] The microscopic Hamiltonian for the graphene sheet is

$$\mathcal{H}=\sum_n t\, c_b^\dagger(\vec{T}_n+\vec{\tau}_b)c_a(\vec{T}_n)+\text{H.c.} \tag{1}$$

where $c_{a(b)}(\vec{R})$ annihilates an electron on the $a(b)$th sublattice at position $\vec{R}$, and the sum is over all the two-dimensional translation vectors $\vec{T}_n$ and over the triad of nearest-neighbor bond vectors $\vec{\tau}_\alpha$ that connect the a and b sublattices.

The Hamiltonian in Eq. (1) is diagonalized by the Fourier transform

$$\begin{pmatrix} c_{a,\vec{k}} \\ c_{b,\vec{k}} \end{pmatrix}=\frac{1}{\sqrt{N}}\sum_{n=1}^{N} e^{i\vec{k}\cdot\vec{T}_n}\begin{pmatrix} e^{i\vec{k}\cdot\vec{d}_a}c_a(\vec{T}_n+\vec{d}_a) \\ e^{i\vec{k}\cdot\vec{d}_b}c_b(\vec{T}_n+\vec{d}_b) \end{pmatrix}, \tag{2}$$

where $\vec{d}_{a(b)}$ locate the $a(b)$ sublattice sites in the unit cell. The spectrum is $E_\pm(\vec{k})=\pm t|\gamma(\vec{k})|=\pm t|\Sigma_\alpha e^{i\vec{k}\cdot\vec{\tau}_\alpha}|$. With one π electron per site the negative energy states are occupied and the Fermi energy lies at $E=0$. Since γ is a complex function of its two-dimensional argument $\vec{k}$, it can vanish only on *discrete points* in reciprocal space. These points correspond to the corners of the two-dimensional Brillouin zone (labeled K and K'). We adopt a ''conventional'' setting of the graphene lattice that places these critical points along the x axis so that $K\equiv(4\pi/3a)(1,0)$ and $K'\equiv-(4\pi/3a)(1,0)$, where a is the graphene lattice constant. In this conventional setting the triad of nearest-neighbor bonds $\vec{\tau}_\alpha$ are $(a/\sqrt{3})\times[(0,1),(\sqrt{3}/2,-1/2),(-\sqrt{3}/2,-1/2)]$.

The low-energy long-wavelength electronic properties of the nanotube are studied by expanding the Hamiltonian (1) around the singular points at the Brillouin zone corners. Near the K point $\vec{k}=\vec{K}+\vec{q}$, and for small q the electronic wave functions $\Psi(\vec{r})$ can be represented by introducing envelope functions $u_K(\vec{r})$ and $v_K(\vec{r})$ that produce a slow spatial modulation of the K point wave functions

$$\begin{aligned}\Psi(\vec{r})&=[\psi_{a,K}(\vec{r})\quad\psi_{b,K}(\vec{r})]\cdot\begin{pmatrix} u_K(\vec{r}) \\ v_K(\vec{r}) \end{pmatrix} \\ &=e^{i\vec{K}\cdot\vec{r}}[U_a(\vec{r})\quad U_b(\vec{r})]\cdot\begin{pmatrix} u_K(\vec{r}) \\ v_K(\vec{r}) \end{pmatrix},\end{aligned} \tag{3}$$

where $U_{a(b)}$ are cell periodic functions localized around the $a(b)$ sublattices

$$U_{a(b)}(\vec{r})\equiv(1/\sqrt{N})\sum_{n=1,N} e^{-i\vec{K}\cdot(\vec{r}-\vec{T}_n-\vec{d}_{a(b)})}f(\vec{r}-\vec{T}_n-\vec{d}_{a(b)}) \tag{4}$$

and $f(\vec{r})$ is a localized basis function.

Introducing the complex notation $q=q_x+iq_y$, $\tau_1=(ia/\sqrt{3})$, $\tau_2=e^{-2\pi i/3}\tau_1=z^*\tau_1$ and $\tau_3=e^{2\pi i/3}\tau_1=z\tau_1$, the Hamiltonian in Eq. (1) is expanded to linear order in q yielding

$$\mathcal{H}_K=\frac{\sqrt{3}ta}{2}\begin{pmatrix} 0 & q_x+iq_y \\ q_x-iq_y & 0 \end{pmatrix}\equiv\hbar v_F(\vec{\sigma}^*\cdot\vec{q}), \tag{5}$$

where σ_μ are the 2×2 Pauli matrices, and $\mathcal{H}_{K'}=-\hbar v_F(\vec{\sigma}\cdot\vec{q})$. Note that these projected Hamiltonians near the K and K' points form an enantiomeric pair of operators that separately break parity, but with opposite handedness.

B. Nanotube effective Hamiltonian

The reduced Hamiltonians $\mathcal{H}_{K(K')}$ are applied to the carbon nanotube by the substitution $qa\rightarrow-ia\nabla$, where the gradient operator acts on the spatial coordinates in the envelope functions u and v. Thus near the K point we obtain the long-wavelength Hamiltonian

$$-i\hbar v_F(\sigma_x\partial_x-\sigma_y\partial_y)\begin{pmatrix} u_K(\vec{r}) \\ v_K(\vec{r}) \end{pmatrix}=E\begin{pmatrix} u_K(\vec{r}) \\ v_K(\vec{r}) \end{pmatrix}. \tag{6}$$

Wrapping the tube along its circumferential direction introduces a subtle quantization condition for the transverse crystal momenta in the envelope functions u_K and v_K. Note that the *physical* electron field Ψ is single valued function of position on the tube, and it is therefore a periodic function of the circumferential coordinate, $\Psi(\vec{r}+\vec{\mathcal{C}})=\Psi(\vec{r})$, where $\vec{\mathcal{C}}$ is the wrapping vector. $\vec{\mathcal{C}}$ is a translation vector of the graphene sheet, and it is conventionally indexed by two integers M and N which define the combination of primitive graphene translations $\vec{a}_1$ and $\vec{a}_2$ that produce a closed orbit on the surface of the nanotube $\vec{\mathcal{C}}=M\vec{a}_1+N\vec{a}_2$. The Bloch phase factor $\exp(i\vec{K}\cdot\vec{r})$ is not a periodic function on the circumference of the tube, since it accumulates a phase $\exp[2\pi i\,\mathrm{mod}(M-N,3)/3]$ on a single closed orbit. Therefore, periodic boundary conditions for Ψ generally require quantization of the crystal momenta in the envelope functions u_K and v_K to *fractional* values, i.e., the fields u_K and v_K are not single valued functions of position on the surface of the tube but instead satisfy the phase-shifted boundary conditions

$$\begin{pmatrix} u_K(\vec{r}+\vec{\mathcal{C}}) \\ v_K(\vec{r}+\vec{\mathcal{C}}) \end{pmatrix}=(z^*)^{\mathrm{mod}(M-N,3)}\begin{pmatrix} u_K(\vec{r}) \\ v_K(\vec{r}) \end{pmatrix}. \tag{7}$$

(The envelope wave functions near the K' point have the conjugate phase shifts $z^{\mathrm{mod}(M-N,3)}$.) Thus u_K and v_K are periodic functions of the tube circumference only for the one-third of the possible wrapped lattices where $\vec{\mathcal{C}}$ is a translation vectors of the $\sqrt{3}\times\sqrt{3}$ superlattice of the graphene sheet. These are special unfrustrated structures for which the zone corner Bloch functions match smoothly around the tube circumference. The other wrapped structures require a phase shift in the envelope functions to continuously match the physical field Ψ around the circumference. It is convenient to impose this boundary condition on u_K and v_K by amending Eq. (6) to include an effective vector potential directed around the tube circumference, and with strength a_m

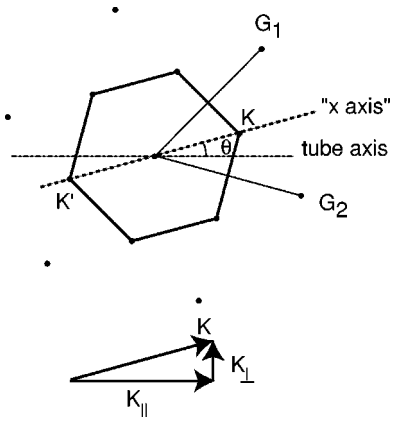

FIG. 1. The x axis of the graphene sheet in its conventional setting can be tipped by an angle θ with respect to the axis of the nanotube. Note that the K point is missaligned with the tube axis in this setting, and has the projections $K_{\|}$ along the tube axis and $K_{\perp}$ along the circumferential direction.

$=(2\pi/\mathcal{C})[m-\frac{1}{3}\mathrm{mod}(M-N,3)]$, where m is an integer index for each of the quantized azimuthal subbands on the nanotube.

Although the projected Hamiltonians $\mathcal{H}_{K(K')}$ are isotropic, the orientation of the graphene lattice in the tangent plane of the tube appear in the theory through the *phases* of their off-diagonal terms. We define the chiral angle θ as an angle between the zone boundary wave vector $\vec{K}$ and the longitudinal axis of the nanotube, as shown in Fig. 1. Using this convention, the projected Hamiltonian Eq. (5) reads

$$\mathcal{H}_K=\frac{\sqrt{3}ta}{2}\begin{pmatrix}0 & (-i\partial_z+ia_m)e^{i\theta}\\ (-i\partial_z-ia_m)e^{-i\theta} & 0\end{pmatrix}, \quad (8)$$

where the partial derivative acts on the electron coordinate z along the axis of the nanotube. Thus for an armchair tube where the conventional x axis of the graphene sheet and the nanotube axis coincide, we have $\theta=0$.

The eigenfunctions of the Hamiltonian in Eq. (8) are Bloch states with reduced crystal momenta q with the dispersion relation

$$E_m(q)=\hbar v_F\sqrt{q^2+\left(\frac{2\pi}{\mathcal{C}}[m-\tfrac{1}{3}\mathrm{mod}(M-N,3)]\right)^2} \quad (9)$$

and with eigenvectors (suppressing the index K)

$$\psi_q(z)=e^{iqz}\begin{pmatrix}u_q\\ v_q\end{pmatrix}=\frac{e^{iqz}}{\sqrt{2}}\begin{pmatrix}e^{-i(\phi+\theta)/2}\\ e^{i(\phi+\theta)/2}\end{pmatrix}, \quad (10)$$

where the phase angle $\phi=\arctan(a_m/q)$ and θ is the chiral angle defined in Fig. 1. Thus the dispersion relation of the graphene sheet is ''sliced'' into hyperbolic branches, with pairs of branches indexed by the azimuthal quantum number m. The $m=0$ branch is gapless for nanotubes with $\mathrm{mod}(M-N,3)=0$. Closer analysis shows that when $\mathrm{mod}(M-N,3)=0$ and $M\neq N$ a small residual gap arises from the broken threefold rotational symmetry in the Hamiltonian due to the tube curvature.[6]

C. Angular momenta in the azimuthal subbands

The eigenstates of the effective mass theory are indexed by their crystal momentum in the tangent plane of the tube or, equivalently, by the z components of crystal momentum and angular momentum. These quantum numbers play a central role in determining the interaction of the tube orbitals with an encapsulated species. Note however that the angular momentum quantum number is generally *not* identical to the azimuthal subband index introduced in the preceding section.

The electron field Ψ can be expanded in the Bloch basis functions $\psi_{a,K}(\vec{r})$ and $\psi_{b,K}(\vec{r})$. The *periodic* parts of these functions can be expressed in the Fourier series $U_\alpha=\Sigma_n[e^{-i\vec{G}_n\cdot\vec{d}_\alpha}F(|\vec{K}+\vec{G}_n|)]e^{i\vec{G}_n\cdot\vec{r}}$, where $F(q)$ is the Fourier transform of the localized orbital $f(\vec{r})$ in Eq. (4). It is isotropic since $f(\vec{r})$ represents a π orbital with orientation perpendicular to the tangent plane of the graphene sheet. Retaining in the sum only the terms with $|\vec{K}+\vec{G}_n|=|\vec{K}|$ (the ''lowest star'' approximation) we find that the physical electron field on the surface of the tube is

$$\Psi(\vec{r})=F(K)\sum_n e^{i(\vec{K}+\vec{G}_n)\cdot\vec{r}}(1,\ e^{-i\vec{G}_n\cdot\vec{\tau}_\alpha})\cdot\begin{pmatrix}u_q\\ v_q\end{pmatrix}e^{i(qz+a_mR\phi)}, \quad (11)$$

where $\vec{r}$ is a vector in the tangent plane of the tube of radius R, z is its axial component and ϕ is the azimuthal angular coordinate around the tube circumference.

Equation (11) demonstrates that the total phase accumulated by the wave function around the tube circumference has contributions from both the subband index m and the phase of the zone boundary Bloch function. The physical angular momenta $\tilde{m}$ are integral and are given by

$$\tilde{m}_n=m_n-\mathrm{int}\left(\frac{M-N}{3}\right)-\frac{1}{2\pi}\vec{G}_n\cdot\vec{\mathcal{C}}_{MN}, \quad (12)$$

where ''int'' is the nearest-integer function. The offset $\mathrm{int}[(M-N)/3]$ in Eq. (20) is smallest for tube wrappings near the armchair $M=N$ geometry and largest for tubes near the zigzag [e.g., $(M,0)$] structures. Note also that the sum in Eq. (11) involves a sum over the *three* members $\vec{K}+\vec{G}_n$ forming a star of K points and thus even in the lowest star approximation, a single azimuthal subband contains an admixture of several different *physical* angular momenta. This mixing results from umklapp processes on the graphene lattice in the tangent plane of the tube. In our calculations below we focus on the element of the star with the smallest values of $\tilde{m}_n$ and denote this value simply as $\tilde{m}$.

These effects are illustrated in Fig. 2 where we display line plots of the real and imaginary parts of Ψ for the lowest $m=0$ azimuthal subbands of the (11,10) and (17,0) nanotubes. Both are oscillating functions of azimuth. However, the (11,0) tube is nearly in the ''armchair'' configuration, and approximately one third of the amplitude in the the $m=0$ subband is found in the $\tilde{m}=0$ state producing a nonzero average value for these fields. By contrast, the lowest m

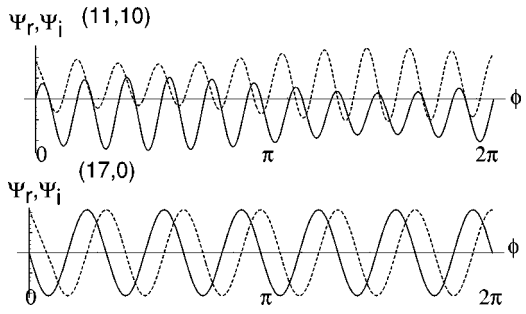

FIG. 2. Wave functions for the lowest azimuthal subbands with $(m=0)$ on an (11,10) and a (17,0) nanotube are plotted as functions of the azimuthal angle ϕ. The plots give the real (solid) and imaginary (dashed) parts of the physical electron field Ψ. For the (17,0) tube the lowest azimuthal subband has an $\tilde{m}=0$ component (note that the average value of Ψ is nonzero). For the zigzag (17,0) tube the smallest angular momentum component occurs for $\tilde{m}=6$ and the average value of Ψ vanishes.

$=0$ subband of the (17,0) tube has a minimum $\tilde{m}=6$ (i.e., there is no $\tilde{m}=0$ component) and it oscillates with an average value of zero.

III. FULLERENE ORBITALS

One can also develop a model for the molecular orbitals of C_{60} using a ''nearly free-electron'' description. In fact, the multiplet structure of the π electron spectrum of the C_{60} molecule immediately identifies these states as free particle states on the surface of a sphere that are split in the icosahedral crystal field of the fullerene molecule.[10] For angular momenta $L>2$ the $2L+1$ fold degeneracy is broken by the discrete rotational symmetry of the molecule. Nevertheless in each angular momentum channel one may construct the symmetrized combinations of the free particle states that transform as irreducible representations of the icosahedral point group. These symmetrized states turn out to provide a good description of the electronic states of the next several orbital multiplets. Of particular interest are the highest unoccupied orbital (HOMO) of the molecule, which is a fivefold degenerate h_u multiplet, and the two lowest unoccupied orbitals (LUMO's) which are three fold degenerate multiplets of t_{1u} and t_{1g} symmetry.

To study these orbitals we diagonalize a tight binding Hamiltonian that connects the nearest-neighbor sites on the surface of the C_{60} molecule. We then compute the overlap of its eigenstates $\Phi_m(\hat{\Omega}_n)$ with the free particle states Y_{LM} projected onto the discrete C_{60} lattice.

$$C_{LM;m}=\frac{\sum_n Y^*_{LM}(\hat{\Omega}_n)\Phi_m(\hat{\Omega}_n)}{\sqrt{\sum_n Y^*_{LM}(\hat{\Omega}_n)Y_{LM}(\hat{\Omega}_n)}}. \tag{13}$$

By this method one finds that the five orbitals of the h_u manifold are derived mainly from the $L=5$ free particle states and transform as a pseudotensor (i.e., they transform as a tensor under spatial rotations, but are odd under spatial inversion). The t_{1u} form a vector representation in the $L=5$ manifold and the t_{1g} states from a pseudovector (odd under rotation, and even under inversion) representation derived from the $L=6$ manifold.

The overlap matrix $C_{LM;m}$ has a simple structure in a geometry where the fivefold symmetry axis of the fullerene molecule is oriented along the z direction. This quantizes the angular momenta about the highest symmetry axis of the molecule. Interestingly, calculations using van der Waals potentials between atomic sites show that the fullerene-nanotube interaction energy is optimized in this geometry.[11] In Tables I–III we display the normalized overlap matrix elements obtained for this orientation. We note that orbital quantization around the fivefold-symmetry axis greatly constrains the possible mixing among the azimuthal components in a given angular momentum channel. Thus, for the t_{1u} orbital the $L=5,M=0$ state can mix with $L=5,M=\pm 5$ states, but the mixing with all other azimuthal components is symmetry forbidden. Note also that among these three multiplets the $M=0$ state is allowed *only* in the t_{1u} vector representation. Thus only the t_{1u} orbital admits an azimuthally isotropic component. This is demonstrated in Fig. 3 where we plot the probability amplitude for the components of the t_{1u} and t_{1g} orbital multiplets that are symmetric under $2\pi/5$ rotations about the fullerene fivefold axis.

IV. COUPLING AND EFFECTIVE INTERACTION

A. Mixing Hamiltonian

In this section we develop a model to describe the mixing of the ball-derived and tube-derived electronic degrees of freedom. Consider the case of coupling to a single encapsulated buckyball located at the origin. The microscopic mixing Hamiltonian has the form $\mathcal{H}_{\rm mix}=\Sigma_{\alpha,n}\Sigma_\beta \mathcal{V}_{\alpha,n;\beta}c^\dagger_{\alpha,n}b_\beta$

TABLE I. Overlap matrix elements $C_{5M;m}$ for the h_u orbitals of the buckyball, ordered by $-2\leqslant m\leqslant 2$ (rows) and $-5\leqslant M\leqslant 5$ (columns). The dots denote entries that are zero by symmetry.

M	-5	-4	-3	-2	-1	0	1	2	3	4	5
$m=-2$				0.680					$0.733i$		
$m=-1$					0.806					$-0.592i$	
$m=0$	0.707					0					0.707
$m=1$		$-0.592i$					0.806				
$m=2$			$0.733i$					0.680			

TABLE II. Overlap matrix elements $C_{5M;m}$ for the t_{1u} orbitals of the buckyball, ordered by $-1 \leqslant m \leqslant 1$ (rows) and $-5 \leqslant M \leqslant 5$ (columns). The dots denote entries that are zero by symmetry.

M	-5	-4	-3	-2	-1	0	1	2	3	4	5
$m=-1$					0.502					$0.865i$	
$m=0$	$0.327i$					0.887					$0.327i$
$m=1$		$0.865i$					0.502				

$+\mathcal{V}^*_{\alpha,n;\beta} b^\dagger_\beta c_{\alpha,n}$, where $c^\dagger_{\alpha,n}$ creates an electron on the αth sublattice in the nth cell of the tube (indexed by a two-dimensional translation vector $\vec{T}_n$) and $b^\dagger_\beta$ creates an electron on the βth site of the buckyball. The $\mathcal{V}$'s are the tunneling matrix elements which will be assumed to vary exponentially with the distance between pairs of sites. We rewrite this microscopic Hamiltonian in terms of the long-wavelength degrees of freedom on the ball and tube by computing matrix elements of $\mathcal{H}_{\rm mix}$ between the tube- and ball-derived states

$$\begin{aligned}
&\langle \Psi_{\rm tube} | \tilde{\mathcal{H}}_{\rm mix} | \Phi_m \rangle \\
&\quad = [u^*(0),\ v^*(0)] \times \Bigg[\sum_n \sum_\beta e^{-i\vec{K}\cdot\vec{T}_n - im'\phi'_n} \\
&\qquad \times \begin{pmatrix} \mathcal{V}_{a,n;\beta} \\ e^{-i\vec{K}\cdot\vec{d}_b} \mathcal{V}_{b,n;\beta} \end{pmatrix} Y_{LM}(\hat{\Omega}_\beta) \Bigg] C_{LM,m} \\
&\quad = [u^*(0),\ v^*(0)] \begin{pmatrix} t_{a,LM} \\ t_{b,LM} \end{pmatrix} C_{LM,m}. \qquad (14)
\end{aligned}$$

Equation (14) expresses the amplitude to hop from the $a(b)$th sublattice in the m'th subband to the mth orbital on the ball.

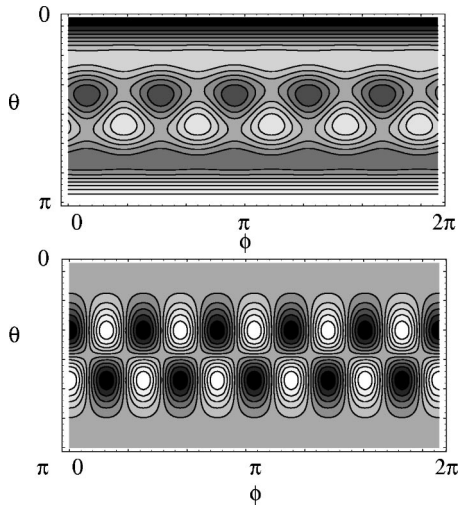

FIG. 3. Contour plots of wave functions from the t_{1u} (top) and the t_{1g} (bottom) orbital multiplets. Both states are invariant under azimuthal rotations of $2\pi/5$. However, note that the t_{1u} state has a nonzero azimuthal average (i.e., it overlaps the $M=0$ free particle state), while the t_{1g} state has zero overlap with the azimuthally isotropic state.

Passing to the continuum limit, the sum in Eq. (14) can be expressed as

$$\begin{aligned}
&\int d^2r' d^2\Omega \sum_{n'} \sum_{L'M'} \gamma_{L'M'} e^{-i(\vec{K}+\vec{G}_{n'})\cdot\vec{r}'_n - im'\phi'_n} \\
&\qquad \times v(|\vec{r}_n - R_b\hat{\Omega}|) Y_{LM}(\hat{\Omega}) Y_{L'M'}(\hat{\Omega}), \qquad (15)
\end{aligned}$$

where $v(r)$ gives the hopping amplitude between atomic sites as a function of their separation. This is assumed to vary exponentially with the separation of the ball coordinate and tube coordinate, $v = \exp(-|\vec{r}'_t - R_b\hat{\Omega}|/a_t)$, where the decay constant $a_t \approx 1$ Å. In the *lowest star* approximation we retain only the reciprocal lattice vectors that connect elements in the first star of K points ($|\vec{K}| = |\vec{K}+\vec{G}_{n'}|$) and the lowest icosahedral harmonic (this is the isotropic term $L'=0, M'=0$). (Since the factor v varies smoothly on the scale of a lattice constant on the surfaces of the tube and buckyball, higher contributions to the sum are suppressed by a form factor.) Thus we consider the overlap integral $\mathcal{O}_{m';LM}$ over the surface of the tube and over the surface of the ball

$$\begin{aligned}
\mathcal{O}_{m';LM} &= \int d^2r'_t \int d\Omega\, e^{-i(\vec{K}+\vec{G}_{n'})\cdot\vec{r}' - im'\phi'_n} \\
&\qquad \times v(|\vec{r}'_t - R_b\hat{\Omega}|) Y_{LM}(\hat{\Omega}) \qquad (16)
\end{aligned}$$

and the bracketed terms in Eq. (14) are therefore

$$\begin{aligned}
\begin{pmatrix} t_{a,LM} \\ t_{b,LM} \end{pmatrix}_{m'} &= \mathcal{P}\mathcal{O}_{m';LM} C_{LM,m} \begin{pmatrix} 1 \\ e^{-i\vec{G}_{n'}\cdot\vec{d}_b} \end{pmatrix} \\
&\propto \mathcal{O}_{m';LM} C_{LM,m} \begin{pmatrix} 1 \\ 1 \end{pmatrix}, \qquad (17)
\end{aligned}$$

where $\mathcal{P}$ is a constant prefactor. Note that it is always possible to define a basis where the relative phase of the tunneling amplitude to the b sublattice is unity.

By expanding the argument of the exponential to quadratic order in the interatomic separations the overlap integral is well approximated by the Gaussian integral

$$\begin{aligned}
\mathcal{O}_{m';LM} &= \frac{2\pi a_t d}{\sqrt{R_b R_t}} e^{-d/a_t} e^{-2a_t d[K_\parallel^2 + (\tilde{m}'^2/R_t R_b)]} \\
&\qquad \times \int d\eta\, e^{iK_\parallel R_b \eta} e^{-(R_b/2a_t)\eta^2} Y_{LM} \\
&\qquad \times (\pi/2+\eta, \phi) e^{-iM\phi} \delta_{M,\tilde{m}'} \\
&= \frac{2\pi a_t d}{\sqrt{R_b R_t}} e^{-d/a_t} e^{-2a_t d[K_\parallel^2 + (\tilde{m}'^2/R_t R_b)]} \mathcal{I}_{LM}. \qquad (18)
\end{aligned}$$

TABLE III. Overlap matrix elements $C_{6M;m}$ for the t_{1g} orbitals of the buckyball, ordered by $-1 \leqslant m \leqslant 1$ (rows) and $-6 \leqslant M \leqslant 6$ (columns). The dots denote entries that are zero by symmetry.

M	-6	-5	-4	-3	-2	-1	0	1	2	3	4	5	6
$m=-1$	$0.379i$					0.788					$0.485i$		
$m=0$		0.707					0					0.707	
$m=1$			$0.485i$					0.788					$0.379i$

Thus we find that the overlap integral requires a Fourier transform of the polar factor of Y_{LM} weighted by a Gaussian peaked at the equator of the ball. The momentum $K_\parallel$ is the projection of the K point wave vector along the tube axis; this depends on the chiral angle of the tube (see the diagram in Fig. 1) and has its maximum value $4\pi/3a \approx 1.70$ Å^{-1} (for an armchair wrapping) and a minimum value $2\pi/\sqrt{3}a \approx 1.47$ Å^{-1} (for a zigzag wrapping). Because of the Gaussian factor the integrand is heavily weighted in the region $|\eta| \leqslant \sqrt{a/R_b} \approx 0.53$. This allows us to obtain a useful approximation to the integral (accurate to $\approx 20\%$) by replacing the momentum by its typical value $K_\parallel \simeq 1.59$ Å^{-1}. We also observe that the overlap integral contains in its exponential prefactor a *form factor* $\exp[-2a_t d(K_\parallel^2 + \tilde{m}'^2/R_t R_b)]$; since this is determined mainly by the magnitude of the wave vector at the K point, it is nearly independent of the tube wrapping vector.

The tunneling amplitudes t are obtained by contracting the overlap matrix elements $\mathcal{I}$ with the amplitudes $C_{LM,m}$ for the mth buckyball orbital, using Eq. (17). The overlap matrix element with the tube orbital selects a single value of the azimuthal quantum number M, and we therefore tabulate the M-resolved tunneling amplitudes for each component of the h_u, t_{1u}, and t_{1g} multiplets in Tables IV–VI. A single azimuthal subband defines a value for the allowed z component of angular momentum $\tilde{m}' = M$ for which the allowed couplings with the ball orbitals (indexed by m) are tabulated in each column of Tables IV–VI. By inspecting these tables we identify the following trends.

(a) The coupling strengths are largest for the smallest values of $|M|$.

(b) Only the t_{1u} orbital couples to an azimuthally isotropic $M=0$ state. This was noticed as a special feature of this orbital in Sec. III. Interestingly we see that the coupling to the $L=5, M=0$ orbital involves the first spatial derivative of the wave function $\partial\Psi/\partial z$ at the impurity site, i.e., the coupling involves the odd component of the Bloch factor $e^{i\vec{K}\cdot\vec{r}}$. The *largest* couplings are obtained in for those tubes in which the $\tilde{m}'=0$ mode couples to the $m=0$ t_{1u} orbitals.

(c) The matrices are ''sparse'' and therefore a given azimuthal subband will have only a few allowed couplings to the buckyball orbitals.

B. Effective tube Hamiltonian

By combining the results of Secs. II B, III, and IV we arrive at a Hamiltonian describing the motion of electrons on the tube, on the ball and their coupling

$$\mathcal{H} = \int dz \frac{\sqrt{3}t}{2} \psi^\dagger(z) \times \begin{pmatrix} 0 & (-i\partial + ia_m)e^{i\theta} \\ (-i\partial - ia_m)e^{-i\theta} & 0 \end{pmatrix} \psi(z) + \sum_m \Phi_m^\dagger E_m \Phi_m + \psi^\dagger(0) \begin{pmatrix} t_{a,m} \\ t_{b,m} \end{pmatrix} \Phi_m + \Phi_m^\dagger (t_{a,m}^*, \; t_{b,m}^*) \psi(0). \tag{19}$$

Here the buckyball is centered at the origin, $\psi(z) = [u(z), v(z)]$ is a two component spinor for the effective mass fields near the K point and Φ_m annihilates the mth buckyball orbital with energy E_m. (Note that a closely related expression describes the coupling to the effective mass fields near the K' point.) To simplify our notation in this section, we suppress the orbital index m and treat the case of single bound orbital on the ball with energy E_o.

By integrating out the buckyball degree of freedom in this Hamiltonian we obtain an energy dependent matrix self-energy acting on the spinor field ψ

TABLE IV. Tunneling amplitudes $t_{a(b);5M}|_m$ for the h_u orbitals of the buckyball, ordered by $-2 \leqslant m \leqslant 2$ (rows) and $-5 \leqslant M \leqslant 5$ (columns). Using Eq. (31) the tunneling amplitudes t_a and t_b are obtained by scaling these numbers with a constant prefactor $\mathcal{P}$. The dots denote entries that are zero by symmetry.

M	-5	-4	-3	-2	-1	0	1	2	3	4	5
$m=-2$				$-0.140i$					$-0.151i$		
$m=-1$					0.155					-0.094	
$m=0$	0.054					0					0.054
$m=1$		-0.094					-0.155				
$m=2$			$0.151i$					$-0.140i$			

TABLE V. Tunneling amplitudes $t_{a(b);5M}|_m$ for the t_{1u} orbitals of the buckyball, ordered by $-1 \leqslant m \leqslant 1$ (rows) and $-5 \leqslant M \leqslant 5$ (columns). Using Eq. (31) the tunneling amplitudes t_a and t_b are obtained by scaling these numbers with a constant prefactor $\mathcal{P}$. The dots denote entries that are zero by symmetry.

M	-5	-4	-3	-2	-1	0	1	2	3	4	5
$m=-1$					0.096					0.138	
$m=0$	$-0.025i$					0.167 i					$0.025i$
$m=1$		0.138					-0.096				

$$\hat{\Sigma}(z,E)=\psi^{\dagger}(z)\begin{pmatrix} t_a^* t_a & t_a^* t_b \\ t_b^* t_a & t_b^* t_b \end{pmatrix}\psi(z)\frac{a\,\delta(z)}{E-E_o} \tag{20}$$

and Eq. (35) is replaced by an effective Hamiltonian on the surface of the tube

$$\mathcal{H}=\int \frac{dz}{a}\frac{\sqrt{3}t}{2}\psi^{\dagger}(z) \times\left[\begin{pmatrix} 0 & a(-i\partial+ia_m)e^{i\theta} \\ a(-i\partial-ia_m)e^{-i\theta} & 0 \end{pmatrix} +\hat{\Sigma}(z,E)\right]\psi(z). \tag{21}$$

The self-energy Σ describes processes in which an electron hops on and off the buckyball at the origin $z=0$, producing a localized potential as seen from the surface of the tube. The matrix self-energy has the structure of a *projection operator* where the spinor state (t_a^*, t_b^*) is scattered by the defect, while the orthogonal state $(t_b, -t_a)$ is perfectly transmitted. For the coupling Hamiltonian derived in the preceding section $t_a=t_b$ and only the sublattice symmetric spinor (1,1) is scattered. This leads to a nontrivial k dependence in the scattering problem that we solve in Sec. V.

The effective potential is energy dependent: attractive for tube states with energies below the on ball resonance $E<E_o$ and repulsive for states with energies $E>E_o$. When tube states ''match'' the on ball self-energy E_o (to a precision given by strength of the tunneling amplitude t) the tube modes can resonate with the encapsulant orbitals and are strongly mixed. Our model ignores any direct hopping motion between neighboring buckyballs that are encapsulated within the nanotube. This is motivated by the experimental data that indicate the effects of hybridizing the buckyball orbitals with the nanotube modes are significantly stronger than the direct coupling between neighboring balls in a peapod lattice.

V. SCATTERING FROM BUCKYBALLS AND BUCKYBALL DIMERS

In this section we formulate and solve the scattering problem for electrons on a nanotube scattering from encapsulated buckyballs in isolation or as isolated dimers. The closely related problem of propagation on a tube with an ordered encapsulated lattice is solved in Sec. VI. We find that most of the important spectral features found for the ordered lattice problem are found at the level of scattering from isolated *dimers* though not from isolated *monomers*. This indicates that the relevant physics for the encapsulated lattice is relatively short ranged in this system. Nonetheless the effects of multiple scattering between neighboring buckyballs must be included to obtain a reasonable description of electronic phenomena in the densely packed phase.

A. Nanotube Green's functions

The equation of motion for the one-electron Green's function $\mathcal{G}(z,z';E)$ is

$$(E-\mathcal{H})\cdot\mathcal{G}(z,z';E)=a\,\delta(z-z'), \tag{22}$$

where a is the graphene lattice constant. In this expression $\mathcal{G}$ is a 2×2 matrix operator that we will calculate explicitly in the *site* representation. In this representation the nanotube Hamiltonian is expressed $\mathcal{H}=-i\hbar v_F\sigma_x(\partial/\partial z)+\delta\sigma_y$ so that the Green's function with outgoing boundary conditions to the left and right of the source at z' is

$$\mathcal{G}(z,z')=-\frac{iae^{iq(z-z')}}{2\hbar v_F\cos\phi}\begin{pmatrix} 1 & \mathrm{sgn}(z-z')e^{-i\phi} \\ \mathrm{sgn}(z-z')e^{i\phi} & 1 \end{pmatrix}. \tag{23}$$

B. Scattering from an isolated encapsulant

Here we use the Green's functions derived in the preceding section to study the electronic spectrum for a nanotube containing a single encapsulated buckyball. Parsing the

TABLE VI. Tunneling amplitudes $t_{a(b);6M}|_m$ for the t_{1g} orbitals of the buckyball, ordered by $-1 \leqslant m \leqslant 1$ (rows) and $-5 \leqslant M \leqslant 5$ (columns). Using Eq. (31) the tunneling amplitudes t_a and t_b are obtained by scaling these numbers with a constant prefactor $\mathcal{P}$. The dots denote entries that are zero by symmetry.

M	-6	-5	-4	-3	-2	-1	0	1	2	3	4	5	6
$m=-1$	$-0.033i$					$0.126i$					$0.079i$		
$m=0$		$0.127i$					0					$0.127i$	
$m=1$			$0.079i$					$-0.126i$					$-0.033i$

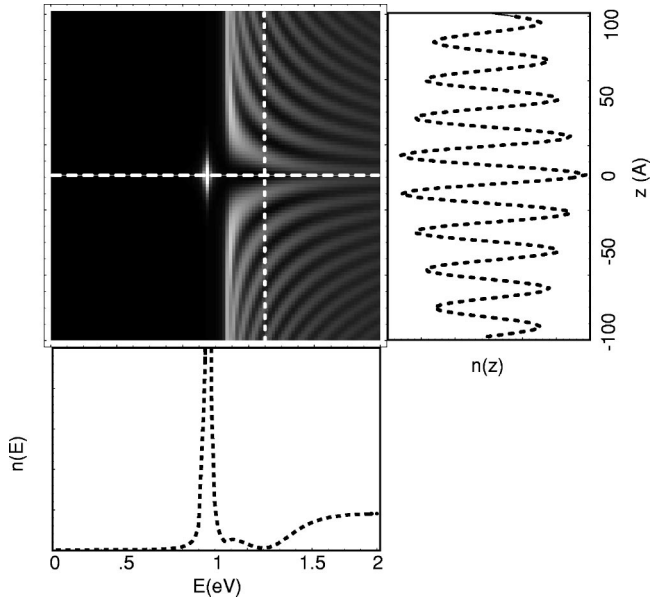

FIG. 4. Density plot of the local density of states $n(z,E)$ on the surface of the nanotube encapsulating a single buckyball. The lineplots give the charge density $n(z)$ and the density of states $n(E)$ along single cuts across the density plot as shown. In this calculation gapped nanotube bands with a gap parameter $\delta=1.1$ eV are mixed with a buckyball orbital with energy $E_o=1.3$ eV with hybridization strength $t=0.9$ eV.

Hamiltonian into an unperturbed piece and a defect potential, $\mathcal{H}=\mathcal{H}_0+\hat{\Sigma}$, we compute the Green's function in the presence of the point scatterer by solving the Dyson equation $\mathcal{G}^{-1}=\mathcal{G}_0^{-1}-\hat{\Sigma}(E)$, where $\mathcal{G}_0^{-1}$ is the bare Green's function and $\hat{\Sigma}(E)=a\Gamma(E)\delta(z)$ with $\Gamma(E)$ containing the energy dependent matrix terms in Eq. (20). $\mathcal{G}(z,z')$ is a 2×2 matrix function of the continuous spatial variables z and z'; inner products are carried out by integrations over z and by summation over the sublattice indices. The self-consistent solution to the Dyson equation yields

$$\mathcal{G}=\begin{pmatrix} \mathcal{T}_0\mathcal{G}_0(0,0) & \mathcal{T}_0\mathcal{G}_0(0,z) \\ \mathcal{G}_0(z,0)\mathcal{T}_0 & \mathcal{G}_0(z,z)+\mathcal{G}_0(z,0)\mathcal{V}\mathcal{T}_0\mathcal{G}_0(0,z) \end{pmatrix}, \quad (24)$$

where $\mathcal{T}_0=[\mathcal{I}_2-\mathcal{G}_0(0,0)\mathcal{V}]^{-1}$. The diagonal elements of the Green's function have a simple interpretation in terms of closed Feynman paths that propagate from some position z to the impurity site $z=0$ where they interact with the defect potential and then return to their original position at z.

To illustrate the effects of scattering from a single encapsulant, in Fig. 4 we collect our results for the local density of states, resolved in energy and position, along the length of a nanotube that surrounds an encapsulant centered at the origin. In this calculation we consider coupling of a single nanotube orbital with energy $E_o=1.3$ eV to azimuthal subbands with gap parameter $\delta=1.1$ eV and hybridization strength $t=0.9$ eV. (These choices turn out to provide a reasonable description of the experimental data for the dense peapod lattice, as detailed below.) The local density of states is obtained from a trace of the Green's function $n(z,E)=-(1/\pi)\mathrm{Im\ tr}\ \mathcal{G}(z,z,E)$ and it is plotted in the gray-scale of the density plot of Fig. 4. The attached line plots give the data on two linescans as a function of energy for fixed position (on top of the defect site) and as a function of position for fixed energy (near the unperturbed energy of the buckyball orbital).

The figure illustrates two important effects. For energies $E<E_o$ the effective potential on the nanotube is attractive, and this produces a bound state on the wall of the nanotube. This state is *not* simply the bound orbital on the buckyball, but rather it arises from strong mixing of the nanotube states with the active orbital on the buckyball. (Note that the data in Fig. 4 are projections of the Green's function onto the tube degrees of freedom.) For energies $E>E_o$ the effective potential on the nanotube is repulsive. We observe that in the position line scan, the electronic density of states exhibits a *minimum* at the defect site. Nevertheless this repulsive potential backscatters the propagating modes of the tube and the interference between the forward and reflected wave produces the standing wave pattern shown in the density plot and in the lineplot to the right. This backscattering mixes propagating states at momenta $\pm q(E)$ and the wavelength of these oscillations is energy dependent with $\lambda=2\pi/2|q(E)|$.

C. Scattering from a bucky dimer

The solution to the scattering problem for a bucky dimer is similar to the treatment given in the preceding section, with the important complication that phase coherence between the scattering processes at the two defect sites now must be included in the calculation. Interestingly, we find that essentially all the features of spectrum of the bucky lattice are found at the level of the scattering theory for the single bucky dimer.

In our model we treat two identical scattering sites at positions $\pm d/2$; $g_{s,s'}$ denotes the various components of $\mathcal{G}_0$ that connect these two sites, i.e., $g_{+-}=\mathcal{G}_0(d/2,-d/2)$. Then the unperturbed Green's function can be written in a block matrix form

$$\mathcal{G}_0=\begin{pmatrix} g_{--} & g_{-+} & \mathcal{G}_0(-d/2,z') \\ g_{+-} & g_{++} & \mathcal{G}_0(d/2,z') \\ \mathcal{G}_0(z,-d/2) & \mathcal{G}_0(z,d/2) & \mathcal{G}_0(z,z') \end{pmatrix}. \quad (25)$$

Thus the inverse of the $\mathcal{T}$ matrix can be reconstructed

$$\mathcal{T}^{-1}=\begin{pmatrix} \mathcal{I}_2-g_{--}\mathcal{V} & -g_{-+}\mathcal{V} & 0 \\ -g_{+-}\mathcal{V} & \mathcal{I}_2-g_{++}\mathcal{V} & 0 \\ -\mathcal{G}_0(z,-d/2)\mathcal{V} & -\mathcal{G}_0(z,d/2)\mathcal{V} & \mathcal{I} \end{pmatrix} \quad (26)$$

and the Green's function in the presence of the pair of scatterers is

$$\mathcal{G}=\begin{pmatrix} \mathcal{T}_{--}g_{--}+\mathcal{T}_{-+}g_{+-} & \mathcal{T}_{--}g_{-+}+\mathcal{T}_{-+}g_{++} & \\ \mathcal{T}_{+-}g_{-+}+\mathcal{T}_{++}g_{+-} & \mathcal{T}_{+-}g_{-+}+\mathcal{T}_{++}g_{++} & \\ & & \mathcal{G}_s(z,z') \end{pmatrix}, \tag{27}$$

where

$$\begin{aligned}\mathcal{G}_s(z,z)&=\mathcal{G}_0+\mathcal{G}_0(z,-d/2)\mathcal{T}_{--}\mathcal{G}_0(-d/2,z)\\&+\mathcal{G}_0(z,-d/2)\mathcal{T}_{-+}\mathcal{G}_0(d/2,z)\\&+\mathcal{G}_0(z,d/2)\mathcal{T}_{+-}\mathcal{G}_0(-d/2,z)\\&+\mathcal{G}_0(z,d/2)\mathcal{T}_{++}\mathcal{G}_0(d/2,z)\\&=\mathcal{G}_0+\sum_{s,s'=\pm}\mathcal{G}_0(z,sd/2)\mathcal{T}_{ss'}\mathcal{G}_0(s'd/2,z).\end{aligned} \tag{28}$$

Each term in the Born series for the external Green's function $\mathcal{G}_s$ describes the amplitude for a closed Feynman path for an electron starting at position z to propagate into the defect region where it is repeatedly scattered within and between the two impurity sites and finally propagates out of the scattering region back to its original position.

In Fig. 5 we collect our results for the hybridization of the nanotube electrons with an isolated encapsulated dimer with a separation $d=10$ Å between the buckyballs. From the density plot and the position line scans it is clear that each buckyball induces a bound state in the nanotube spectrum. These are mixed to produce a ''bonding'' and ''antibonding'' combination. The position line scans pass through the energies of these two bound states, and show a zero in the density of the antibonding states at the midpoint of the dimer. Note that in this calculation there is *no* direct mixing between the buckyball orbitals; rather the splitting is completely due to indirect mixing by coupling to the tube degrees of freedom.

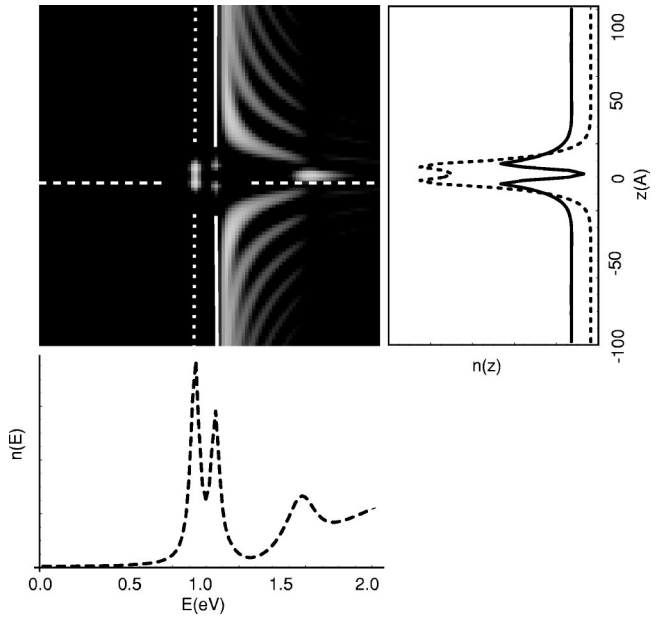

FIG. 5. Density plot of the local density of states $n(z,E)$ on the surface of the nanotube encapsulating an isolated buckyball dimer. The separation between buckyballs in the dimer $d=10$ Å. The line-plots give the charge density $n(z)$ and the density of states $n(E)$ along single cuts across the density plot as shown. In this calculation gapped nanotube bands with a gap parameter $\delta=1.1$ eV are mixed with buckyball orbitals with energy $E_o=1.3$ eV with hybridization strength $t=0.9$ eV.

At energies just above the gap $E>\delta$ the hybridization of the tube and ball degrees of freedom produces a deep mimimum in the local density of states seen on the tube. At higher-energy $E\approx 1.6$ eV we see an enhancement of electron density at the midpoint of the dimer. This arises from a Fabry-Perot type resonance. Here incident electronic waves are multiple reflected from each defect site, and at this energy the wavelength of the Bloch states is ''matched'' to the interdefect spacing. Thus, we find that below the orbital energy E_o the electronic density on the tube is enhanced on the defect sites, whereas above E_o the electronic density is enhanced between the defect sites.

VI. KRONIG PENNEY MODEL

In this section we apply the model developed in Sec. V to an ordered array of encapsulated fullerenes, a ''fullerene peapod.'' The discrete translational symmetry of this structure leads to the formation of electronic bands in which the nanotube and buckyball degrees of freedom are hybridized. The Hamiltonian for an ordered array of encapsulated peapods is

$$\mathcal{H}=-i\hbar v_F\sigma_x\partial_z+\delta\sigma_y+a\Gamma(E)\sum_n\delta(z-na_b), \tag{29}$$

where the σ's are Pauli matrices and a_b is the interball spacing. Since the scattering potential in Eq. (29) is periodic, with superlattice period a_b its eigenfunctionscan be chosen to satisfy Bloch boundary conditions $\psi_k(z)=e^{ikz}U_k(z)$, where the function $U_k(z)$ is a spinor field that is periodic, obeying the boundary condition $U_k(z+a_b)=U_k(z)$. In the domain $0<z<a_b$, the electron states at energy E aresuperpositions of the free particle states $\psi_k(z)=A\psi_+(z)+B\psi_-(z)$ and U_k is therefore explicitly

$$\begin{aligned}U_k(z)&=\begin{pmatrix} e^{-i\phi/2} & e^{i\phi/2}\\ e^{i\phi/2} & -e^{-i\phi/2}\end{pmatrix}\begin{pmatrix} e^{i(q-k)z} & 0\\ 0 & e^{-i(q+k)z}\end{pmatrix}\begin{pmatrix} A\\ B\end{pmatrix}\\&=\mathcal{U}\cdot\begin{pmatrix} e^{i(q-k)z} & 0\\ 0 & e^{-i(q+k)z}\end{pmatrix}\begin{pmatrix} A\\ B\end{pmatrix},\end{aligned} \tag{30}$$

where $\hbar v_F q=\sqrt{E^2-\delta^2}$ and $\phi=\arctan\delta/\sqrt{E^2-\delta^2}$. [Recall that for nonzero chiral angle, θ, the phase angle $\phi\rightarrow\phi+\theta$, using Eq. (8).]

The Bloch wave vector k and the expansion coefficients A and B are obtained by integrating around the singular δ-function scattering potential at $z=0$ yielding the matching condition

$$\left(-i\hbar v_F\sigma_x[\psi_k(0^+)-\psi_k(0^-)]+\frac{a\Gamma(E)}{2}(\psi_k(0^+)+\psi_k(0^-))\right)=0. \tag{31}$$

This is cast in the form of a conventional eigenvalue problem by the rearrangment

$$\begin{aligned}\mathcal{U}\cdot\begin{pmatrix}e^{-iqz}&0\\0&e^{iqz}\end{pmatrix}\mathcal{U}^{-1}\cdot\left(i\hbar v_F\sigma_x+\frac{a\Gamma(E)}{2}\right)^{-1}&\\ \times\left(i\hbar v_F\sigma_x-\frac{a\Gamma(E)}{2}\right)\cdot\mathcal{U}\begin{pmatrix}A\\B\end{pmatrix}&\\ =\begin{pmatrix}e^{-ikz}&0\\0&e^{-ikz}\end{pmatrix}\cdot\mathcal{U}\begin{pmatrix}A\\B\end{pmatrix}&\end{aligned} \tag{32}$$

or, introducing a more compact notation

$$\mathcal{U}\mathcal{P}_q\mathcal{U}^{-1}\cdot\mathcal{S}(E)\cdot\mathcal{U}\begin{pmatrix}A\\B\end{pmatrix}=e^{-i\theta_k}\mathcal{U}\begin{pmatrix}A\\B\end{pmatrix}. \tag{33}$$

Equation (33) has a simple interpretation. The vector

$$\begin{pmatrix}\alpha\\\beta\end{pmatrix}=\mathcal{U}\begin{pmatrix}A\\B\end{pmatrix} \tag{34}$$

expresses the eigenvectors of this problem rotated from the running wave representation into the sublattice representation. $\mathcal{U}\mathcal{P}_q\mathcal{U}^{-1}$ is the free particle propagator in this basis, and $\mathcal{S}(E)$ is the phase-shift accrued by scattering through an impurity site. Equation (33) tells us to choose α and β to find the linear combination of free running waves of the unperturbed problem that satisfy Bloch boundary conditions in the presence of scattering from the impurity lattice.

The hybridizated electronic spectrum for the fullerene peapod is plotted in Fig. 6. The dashed curves give the unmixed spectra for the gapped bands of the nanotube and the localized orbitals on the buckyballs. Note that in this approximation the buckyball band is perfectly dispersionless, i.e., there is no direct hopping between the fullerene sites. Introducing the mixing [formally turning on the self-energy in Eq. (29)] produces and avoided crossing between these branches. This leads to the hybridized bands given by the solid curve. Thelowest band is derived from the bound states produced by the attractive defect potential. It is separated by an energy gap (a *hybridization gap*) from the spectrum of strongly dispersive states. Finally, since the defect potential is periodic with superlattice period a_b, *Bragg gaps* are generated at the zone center ($q=0$) and zone boundaries ($q=\pm\pi/a_b$).

It is interesting that the mixing between the localized ball orbital and the dispersive tube band is not symmetric under the the operation $q\rightarrow -q$. This asymmetry does not violate Kramers theorem since the time reversed partner to the state with crystal momentum q near the K point is a state with crystal momentum $-q$ near the K' point. The source of the asymmetry can be understood by rotating the matrix self-energy back to the basis of propagating tube modes obtained at energy E. This gives a self-energy proportional to

$$\tilde{\Gamma}\propto\mathcal{U}^{\dagger}\cdot\begin{pmatrix}1&1\\1&1\end{pmatrix}\cdot\mathcal{U}=\begin{pmatrix}1+\cos(\phi+\theta)&i\sin(\phi+\theta)\\-i\sin(\phi+\theta)&1-\cos(\phi+\theta)\end{pmatrix}, \tag{35}$$

where $\phi=\arctan(\delta/\sqrt{E^2-\delta^2})$ and θ is the chiral angle. For example, in the ungapped bands of an armchair tube $\phi=0$ and $\theta=0$; thus a hybridization gap opens *only* in the $q>0$ branch, and there is no backscattering. (Near the K' point the situation is reversed, and the hybridization is allowed only in the $q<0$ branch.) Physically this occurs because the propagating modes of the armchair tube are pure ''bonding'' and ''antibonding'' combinations of the A and B sublattice basis functions. The antibonding combination is annihilated by the self-energy operator and so the defect site is ''invisible'' for this combination. For a general chiral angle, or for the gapped electronic bands of a metallic tube, the states at wave vectors $\pm q$ are complex; so that they are neither pure ''bonding'' nor ''antibonding'' in character. Nonetheless, in general the left moving and right moving modes admix with the impurity state with different strengths.

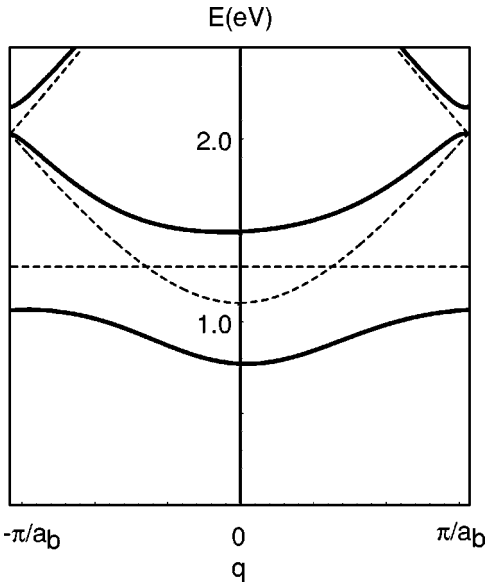

FIG. 6. Scheme for hybridizing the localized mode of a buckyball with the gapped propagating bands of a nanotube. The unmixed bands are given by the dashed curves and the mixed bands are the solid curves. In this calculation gapped nanotube bands with a gap parameter $\delta=1.1$ eV are mixed with buckyball orbitals with energy $E_o=1.3$ eV with hybridization strength $t=0.9$ eV.

Once the eigenvector amplitudes α and β are obtained from Eq. (34), we invert Eq. (30) to find an expression for the charge density

$$\rho_k(z) = (\alpha^* \quad \beta^*) \cdot \begin{pmatrix} 1 & ie^{-2iqz}\sin(\phi+\theta) \\ -ie^{2iqz}\sin(\phi+\theta) & 1 \end{pmatrix} \cdot \begin{pmatrix} \alpha \\ \beta \end{pmatrix}. \tag{36}$$

The tunneling density of states is obtained from the trace of the imaginary part of the single-particle Green's function:

$$\mathcal{G}_{\mu\nu}(z,z';E) = \frac{a}{2\pi}\int dk \frac{\psi_\mu^*(z)\psi_\nu(z')}{E - E(k) + i\epsilon} \tag{37}$$

and is calculated by linearizing the denominator around its zero crossings $\partial E/\partial k|_{k(E)}[k-k(E)]+i\epsilon$. Thus the tunneling density of states $n(E)$ is expressed as

$$n(z,E) = \sum_k \frac{\rho_k(z)}{|\partial E/\partial k|}_{k(E)}. \tag{38}$$

Since the scattering problem is not symmetric under the inversion $k \rightarrow -k$ the sum in Eq. (38) cannot be factored into an energy dependent term multiplied by a spatially varying term (as it would for a symmetric bandstructure).

The effect of the periodic structure of the peapod lattice on the electronic spectrum is apparent in the density plots of the local density state shown in Fig. 7. The impurity states induced by the encapsulants generate an impurity *band*, here extending from ≈ 0.8 eV–1.0 eV. The charge density on the surface of the tube for this band is peaked at the defect sites. This is seen in the linescans on the right which exhibit an ''upward'' cusp in the local density of states at the defect sites. Note also that the top of the impurity band is ''antibonding'' in character, with nodes (i.e., not simply local minima) at the midpoints between neighboring encapsulants. This impurity band is separated from the spectrum of scattering states by a hybridization gap. At energies above the hybridization gap, the character of the charge density is reversed. Here the the local maxima are found in the bond centers between the neighboring encapsulant sites. This is the periodic analog of the Fabry-Perot enhancement of the charge density in the midbond observed for the isolated dimer.

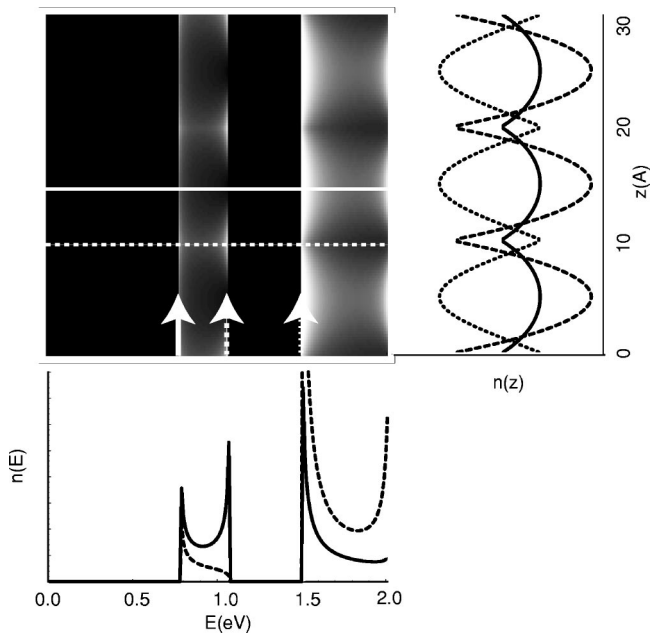

FIG. 7. Density plot of the local density of states $n(z,E)$ on the surface of the nanotube encapsulating a lattice of buckyballs. The separation between buckyballs $d=10$ Å. The lineplots give the charge-density $n(z)$ and the density of states $n(E)$ along single cuts across the density plot as shown. In this calculation gapped nanotube bands with a gap parameter $\delta=1.1$ eV are mixed with buckyball orbitals with energy $E_o=1.3$ eV with hybridization strength $t=0.9$ eV.

VII. COMPARISON WITH EXPERIMENT

The theory of the electronic structure of peapods developed in this paper can be compared to STM measurements on isolated peapods.[9] In these experiments it was found that peapods could be distinguished from unfilled SWNT's by a periodic modulation in the STM topographs that are superimposed on the atomic lattice of the SWNT cage. For an ordered peapod these modulations exhibited an average period of 10 Å, in good agreement with TEM observations of the C_{60} spacing in densely packed peapods.[8] More detailed information about the density of states was obtained from spatially resolved spectroscopic maps made by recording the differential conductance (dI/dV) of the STM junction as a function of the bias voltage V while moving the tip across the top of the peapod.

Figure 8, previously reported in Ref. 9, shows one such spectrosocopic map for an ordered peapod. For this sample the occupied electronic states imaged at negative bias appear to be similar to those expected for an unfilled semiconducting SWNT. The onset of conduction at negative bias for this peapod occurs near -0.5 eV which we interpret as tunneling into the *second* occupied azimuthal subband of a semiconducting SWNT cage with a radius $R \approx 7$ Å. The low tunneling currents at low voltages in this measurement reduce the contribution from first azimuthal subband with an expected onset near -0.25 eV. There is a faint position dependent modulation in the spectroscopic map that can be attributed to small variations in the tip sample separation due to the feedback conditions used in this measurement.[9]

In contrast to the occupied electronic states which are nearly identical to those of an unfilled tube, the unoccupied states, imaged at positive bias, show dramatically different electronic features. After the initial onset of the second SWNT azimuthal subband, the differential conductance shows a strong double peaked modulation with the same periodicity as the encapsulated C_{60} molecules (≈ 10 Å) in the range 1.0–1.25 eV. At higher energies we observe a broad suppression of the differential conductance followed by a second strong onset of conductance near 2.0 eV. A

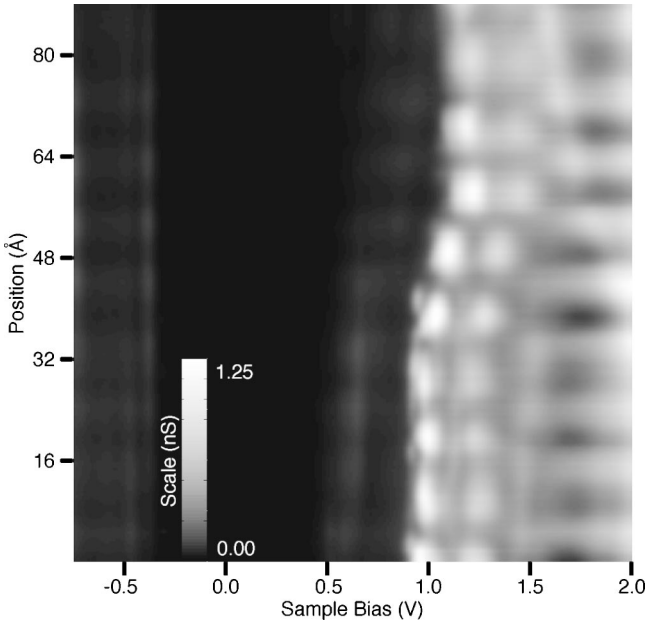

FIG. 8. Spectroscopic map of a fullerene peapod giving a density plot of the spatially resolved differential tunneling conductance measured as a function of sample bias (horizontal axis) and position (vertical axis).

striking feature of these data is that the modulations of the differential conductance in the low-energy band (1.0–1.25 eV) is *out of phase* with modulated features observed for energies >1.5 eV.

Closer examination of the experimental data shows that the spectral features in the unoccupied density of states slowly shift in energy along the length of the peapod, so that their positions varies by nearly 200 meV. We believe that these spatial variations in the conductance of a SWNT are unrelated to the encapsulated molecules, and are more likely associated with extrinsic effects such as torsion or strain[6,13,14] or possibly simply the trapping of extrinsic charge at defect centers in the sample or the substrate. Note that the periodic encapsulant derived features shift ''rigidly'' with the band onsets in this spectrograph.

The observation of energy dependent periodic variations in the STM spectra demonstrates that the fullerene peapod has an electronic structure that is quite different from that of the unfilled SWNT, as found in the theoretical results presented in Secs. V and VI. A closer comparision of the experimental data with the theoretical results for a peapod lattice is presented in the density plots of Fig. 9.

The agreement between theory and experiment allows us to make assignments of the prominent features in the experimental spectra. The most dramatic feature in the experimental spectrograph is the doublet features at 1.0 and 1.25 eV, which we identify with the extrema of the encapsulant derived impurity band found in the calculations. The region of suppressed differential conductance up to ≈ 1.4 eV indicates the formation of a hybridization gap that separates the impurity band from the next band of propagating states on the SWNT cage. Finally, above the hybridization gap the density modulations are observed to be out of phase with those

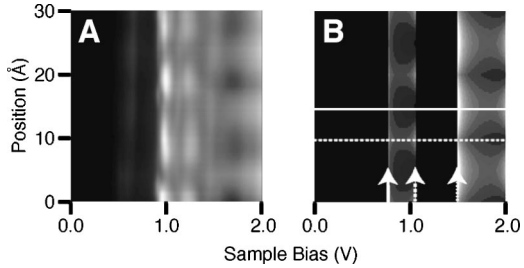

FIG. 9. Comparison of a section of the experimental data from Fig. 8 with the calculated local density of states reproduced from Fig. 7. In the theory a single molecular orbital on the C_{60} with an energy $E_o=1.3$ eV hybridizes with a single azimuthal subband of the SWNT with a band-gap $\delta=1.1$ eV and with a hybridization strength $t=0.9$ eV. The lines and arrows denote the trajectories for the five linescans of the theoretical data shown in Fig 7.

found in the impurity band. This is striking evidence for the formation of the standing wave patterns expected just above and below an electronic band-gap produced by a periodic one-dimensional potential.

VIII. DISCUSSION

The hybridization model developed in Secs. V and VI provides a good description of many aspects of the experimental data. However, there are aspects of the data that are not completely explained by this model, and some predictions of theory that have not yet been observed in experiment. In this section we comment briefly on these remaining discrepancies.

The thresholds for various features in the differential tunneling conductance identifies the host nanotubes as *semiconductors* in which the hybridization is occuring in the *third* azimuthal subband. The gap parameters δ_m for the azimuthal subbands of a nanotube of radius R are $\delta_m=(\hbar v_F/R)\epsilon_m$, where $\epsilon_m=\pm 1/3, \mp 2/3, \pm 4/3$, etc. for semiconducting tubes. For nanotubes with radius ≈ 7 Å the first three subbands have gap parameters $|\delta_m|=0.26, 0.52$, and 1.03 eV, and the second threshhold at ≈ 0.5 eV is clearly resolved in the measured conductance. A C_{60} molecule nests nicely within such a nanotube leaving a typical graphene van der Waals gap between the ball and the wall. Thus, the fundamental premise of the model is that a single azimuthal subband of the nanotube hybridizes with a single molecular orbital of the encapsulated fullerene.

To date the effects of the encapsulant have been observed in the conductance spectra only for *positive* sample bias, i.e., for tunneling electrons from the tip into the peapod, and only into peapods with a semiconducting SWNT cage. It is natural to try to interpret these trends in terms of a ''selection rule'' that constrains the hybridization of the tube- and ball-derived electronic states.

In Table IX we collect some relevant structral and electronic parameters of candidate encapsulating tubes. Here we have compiled data for all tubes that can encapsulate a buckyball with an interwall spacing (between the ball and the wall) 3.0 Å$<d<$3.6 Å. The table gives the value of the interwall spacing, the reduced gap parameters and the z com-

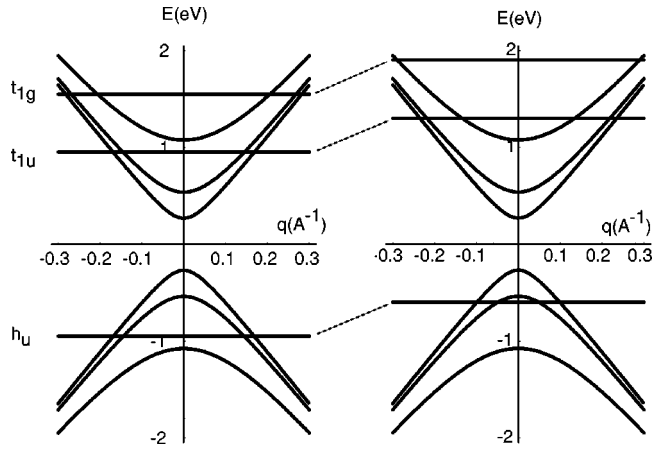

FIG. 10. Hybridization scheme for three lowest dispersing subband pairs of a semiconducting tube coupled with the three dispersionless frontier orbitals of a C_{60} lattice. The symmetries of the C_{60} molecular orbitals are indicated. The level separations of the molecule are taken from a tight binding model for π electrons on the buckyball, with a nearest-neighbor hopping amplitude $t=2.5$ eV. In the left panel the HOMO and LUMO are positioned symmetrically around the gap center. Better agreement with experiment is obtained if the molecular spectrum is shifted by $+0.35$ eV, an effect that could be attributed to orthogonalization to the basis states on the encapsulating carbon nanotube.

ponent of the angular momentum for each azimuthal subband. Ten of the fifteen tubes in this table are semiconductors.

The third gapped azimuthal subband of the semiconducting tubes have reduced gap parameters $\epsilon_m=\pm 4/3$ in this table. For five of the ten semiconducting tubes in this table the z component of the angular momentum matches that of one of the t_{1u} orbitals. These candidate tubes are indexed (12,8), (13,6), (14,6), (15,4), and (17,1). Of this group the prime candidates for those that have been measured experimentally are the tubes with strong coupling to the t_{1u} manifold, namely, the (12,8) and (13,6) wrappings. For the (12,8) tube the third ''conduction band'' of the tube (near the K point) hybridizes the $\tilde{m}=0$ orbital of the t_{1u} multiplet while for the (13,6) tube it hybridizes the $\tilde{m}=-1$ orbital of the t_{1u} multiplet.

The band diagrams in Fig. 10 suggest two plausible scenarios for the *absence* of encapsulant induced structure in the valence states. On the left hand side the HOMO and LUMO are positioned symmetrically about the band center as one might expect by naively equating the chemical potentials of the tube and buckyball lattices. Then, if the hybridzation proceeds through the $\tilde{m}=0$ mode, as required for the (12,8) tube, the coupling is allowed (and strong) for the t_{1u} orbital and *forbidden* for the h_u manifold (i.e., there is no $\tilde{m}=0$ component in the *pseudotensor* h_u manifold. A second scenario is outlined in the right-hand panel. In this case the molecular spectra have been shifted rigidly by $+0.35$ eV. Here the t_{1u} orbital overlaps the third azimuthal subband, a situation that we found provides a good description of the experimental data, and the h_u orbital overlaps the second azimuthal subband in the valence band. For the (13,6) tube the angular momenta of the bands are $\tilde{m}=-1$ (third conduction band) and $\tilde{m}=-3$ second valence band. Inspecting Tables VI and VII we find that the hybridization is again symmetry allowed for the t_{1u} orbital and forbidded for the h_u orbital. It is also interesting that the (13,6) structure has one

TABLE VII. Structural and electronic parameters for fifteen nanotubes that can encapsulate C_{60} with interwall spacings 3.00 Å$<d<$3.6 Å. The tubes are labeled by their wrapping indices (M,N) and only one member of an enantiomeric pair is tabulated [i.e., only (12,8) and not (8,12)]. The data give the tube radius (R) the gap between the fullerene and tube wall (d), the reduced gap parameters (ϵ_m) for the three lowest subbands, and the z component of the angular momenta in these subbands $(\tilde{m})$. The the electronic gap $\delta=\hbar v_F|\epsilon_m|/R$. The entries in the last three columns are negated for the enantiomeric partner.

(M,N)	R(Å)	d(Å)	$\epsilon_{-1}(\tilde{m}_{-1})$	$\epsilon_0(\tilde{m}_0)$	$\epsilon_1(\tilde{m}_1)$
(10,10)	6.78	3.26	$-1(-1)$	0 (0)	1(1)
(11,9)	6.79	3.27	$-4/3(-2)$	$-1/3(-1)$	2/3(0)
(12,7)	6.52	3.00	$-4/3(-3)$	$-1/3(-2)$	$2/3(-1)$
(12,8)	6.83	3.31	$-2/3(-2)$	$1/3(-1)$	4/3(0)
(13,6)	6.59	3.07	$-2/3(-3)$	$1/3(-2)$	$4/3(-1)$
(13,7)	6.88	3.36	$-1(-3)$	$0(-2)$	$1(-1)$
(14,5)	6.69	3.16	$-1(-4)$	$0(-3)$	$1(-2)$
(14,6)	6.96	3.44	$-4/3(-4)$	$-1/3(-3)$	$2/3(-2)$
(15,3)	6.54	3.02	$-1(-5)$	$0(-4)$	$1(-3)$
(15,4)	6.79	3.27	$-4/3(-5)$	$-1/3(-4)$	$2/3(-3)$
(16,2)	6.69	3.17	$-4/3(-6)$	$-1/3(-5)$	$2/3(-4)$
(16,3)	6.93	3.41	$-2/3(-5)$	$1/2(-4)$	$4/3(-3)$
(17,0)	6.66	3.14	$-4/3(-7)$	$-1/3(-6)$	$2/3(-5)$
(17,1)	6.86	3.34	$-2/3(-6)$	$-1/3(-5)$	$4/3(-4)$
(17,2)	7.08	3.56	$-1(-6)$	$0(-5)$	$1(-4)$

of the smallest gap spacings between the ball and the tube of any of the structures tabulated. Thus any symmetry allowed coupling should be particularly strong for this nanotube. Note also, that by inspecting the data of Table VII we predict that certain tubes (e.g., a (12,7) wrapping) *do* have symmetry allowed couplings to buckyball orbitals in the h_u multiplet. None of these have yet been measured experimentally.

Large modulations of the charge density, as are seen in the experiments, suggest that encapsulant orbitals are hybridized with tube states near the subband extrema. The reason for this is contained in Eq. (35) giving the forward and backscattering amplitudes between the propagating tube states at $\pm q$ as a function of the mixing angle ϕ and the tube's chiral angle θ. For the ungapped band of an armchair tube $\phi=0$ and $\theta=0$ so that backscattering is symmetry forbidden, and in this case there is no modulation of the charge density seen on the tube wall in response to the defect potential. For other tube geometries the largest chiral angle entering the theory is quite small ($\theta=\pi/6$, for a zigzag tube), so that whenever $\delta \ll E$ defect induced modulations of the charge density are very small, though not completely absent. For example the chiral angles for the (12,8) and (13,6) tubes are 6.6° and 12° and the charge-density modulations $\Delta\rho/\rho \sim 10^{-2}$ and 4×10^{-2}, respectively when $E \gg \delta$. Thus we expect that the encapsulant can produce significant fluctuations in the charge density of the tube only in the special situation where the resonant molecular levels are well matched in energy to the subband threshholds. It is interesting that this fact alone (beside from any of the symmetry selection rules) favors the hybridization scheme shown in the right panel of Fig. 10.

We speculate that this is the reason for the absence of encapsulant-derived structure in peapods containing metallic nanotubes. Two schematic dispersion relations for this situation are shown in Fig. 11. In the left-hand panel the buckyball molecular orbitals are positioned symmetrically around the band center. Here density fluctuations due to hybridization of the impurity with the ungapped bands should be reduced by the suppression of backscattering as noted above. However, the situation found in the theoretical calculations of Okada *et al.*[15] is better described with the diagram on the right. Here the t_{1u} orbital has shifted to near the Fermi energy, a situation that could be due to a small but nonzero charge transfer onto the buckyball. In this situation the next unoccupied orbital overlaps only the ungapped bands of the conducting tube, and the h_u orbital is resonant with states deep in the valence band where it would be difficult to detect by ordinary scanning tunneling spectroscopy.

The pseudoselection rules derived in this paper apply only to the case where the high symmetry axis of the buckyball aligns with the axis of the nanotube. This configuration are favored energetically within a van der Waals model for the ball-tube interaction. However, other orientations are very likely accessible above a crossover temperature in the 200°–300° K range. Here the encapsulated buckyballs would be expected to resonate with the propagating modes of *any* encapsulating tube. Thus a qualitative temperature dependent change in the conductance spectra for tubes that are ''silent'' in their orientationally ordered low-temperature states would be an important indicator of the interplay of the

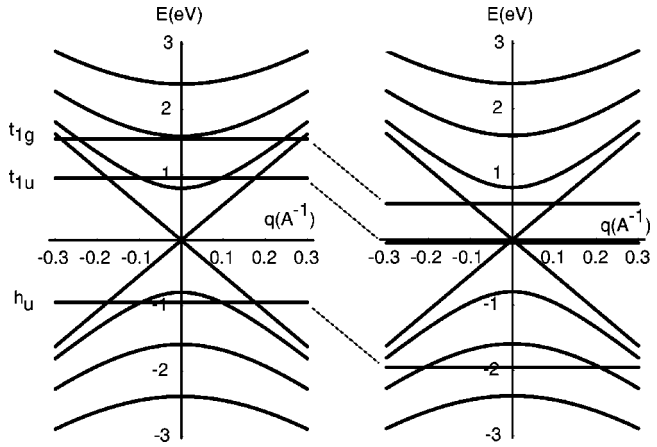

FIG. 11. Hybridization scheme for three lowest dispersing subband pairs of a conducting tube coupled with the three dispersionless frontier orbitals of a C_{60} lattice. The symmetries of the C_{60} molecular orbitals are indicated. The level separations of the molecule are taken from a tight binding model for π electrons on the buckyball, with a nearest-neighbor hopping amplitude $t=2.5$ eV. In the left panel the HOMO and LUMO are positioned symmetrically around the band center. Better agreement with the theoretical calculations of reference 20 is obtained if the molecular spectrum is shifted by -0.95 eV, an effect that could be attributed to charge transfer from the tube onto the ball. The theory of reference 20 also suggests a crystal field splitting of the t_{1u} manifold that is not included in this figure.

hybridization amplitudes and orientation of the encapsulant.

The data reported in Ref. 9 and in this paper are the first direct measurements of the electronic spectra produced by scattering from an encapsulated species. More data of the type presented in Figs. 8 and 9 from measurements on many samples will be needed to verify the predicted sensitivity to the geometric structure, and to examine how these results can be generalized to a larger family of encapsulated stuctures. It is also useful to obtain additional measurements of the electronic spectra for isolated encapsulated buckyballs and buckyball clusters. There are three additional lines of investigation that seem particularly promising for exploring the interaction of propagating modes on the tube walls with various encapsulated species.

(1) Measurements of the differential conductance for isolated encapsulated buckyballs and buckyball dimers can be used to verify the predicted scattering spectra presented in Figs. 4 and 5. A direct measurement of the energy dependence of the modulation wavelength in the charge-density provides a real space image of the coherent backscattering of Bloch waves from a localized encapsulated impurity. The observation of a resonant peak on the tube midway between the encapsulated scatterers in an isolated dimer would provide a striking confirmation of the Fabry-Perot resonance predicted in these calculations.

(2) A fullerene peapod can be electrostatically gated to shift the Fermi energy into the energy region near the hybridization gap. Scattering effects are strongest in this region of the spectrum so that conductance measurements at low bias in this gated geometry can be used to measure the interaction

of the propagating cage modes with the encapsulant. In principle such a measurement can be used to quantify the energy dependence of the transmission coefficient along a single fullerene peapod.

(3) For an undoped peapod, optical excitation of free carriers into states near the hybridization gap can provide important information about the dynamics for hot electrons in states that are strongly hybridized with the encapsulant. In general, studying transients produced by pulsed laser excitation and even attempting coherent optical control of electronic excitations in highly ordered nanoscale systems such as these can provide a unique and largely unexplored window on the carrier dynamics.

ACKNOWLEDGMENTS

Work at the University of Pennsylvania was supported by the Department of Energy under Grant No. DEFG-02-ER0145118 (EJM), by the National Science Foundation under MRSEC Grant No. DMR-00-7990 (C.L.K., A.T.J., D.E.L., and E.J.M.) and by the Office of Naval Research under Grant No. N00014-00-1-0482 (D.E.L.). Work at the University of Illinois at Urbana-Champaign (A.Y.) was supported by NSF CAREER Program (Grant DMR 98-75565), the Department of Energy through the Frederick Seitz Materials Research Laboratory (Grant No. DEFG-02-96ER4539), by the Petroleum Research Fund of the American Chemical Society, and by a Sloan Research Fellowship.

[1] S. Iijima, Nature (London) **354**, 56 (1991).
[2] M.S. Dresselhaus, G. Dresselhaus, and P.C. Eklund, *Science of Fullerenes and Carbon Nanotubes* (Academic Press, New York, 1996).
[3] N. Hamada, S. Sawada, and A. Oshiyama, Phys. Rev. Lett. **68**, 1579 (1992).
[4] J.W. Mintmire, B.I. Dunlap, and C.T. White, Phys. Rev. Lett. **68**, 631 (1992).
[5] R. Saito, M. Fujita, G. Dresselhaus, and M.S. Dresselhaus, Appl. Phys. Lett. **60**, 2204 (1992).
[6] C.L. Kane and E.J. Mele, Phys. Rev. Lett. **78**, 1932 (1997).
[7] A. Bachtold, P. Hadley, T. Nakanishi, and C. Dekker, Science **293**, 76 (2001).
[8] B.W. Smith, M. Monthioux, and D.E. Luzzi, Nature (London) **396**, 323 (1998).
[9] D.J. Hornbaker, S.J. Kahng, S. Misra, B.W. Smith, A.T. Johnson, E.J. Mele, D.E. Luzzi, and A. Yazdani, Science **295**, 828 (2002).
[10] R. Friedberg, T.D. Lee, and H.C. Ren, Phys. Rev. B **46**, 14 150 (1992).
[11] C.L. Kane and E. J. Mele (unpublished).
[12] A.A. Maarouf, C.L. Kane, and E.J. Mele, Phys. Rev. B **61**, 11 156 (2000).
[13] M. Buongiorno Nardelli and J. Bernholc, Phys. Rev. B **60**, R16 338 (1999).
[14] A. Rochefort, D.R. Salahub, and Ph. Avouris, Chem. Phys. Lett. **297**, 45 (1998).
[15] S. Okada, S. Saito, and A. Oshiyama, Phys. Rev. Lett. **86**, 3835 (2001).